Accuracy verification of infrared marker-based dynamic tumor-tracking irradiation using the gimbaled x-ray head of the Vero4DRT (MHI-TM2000)

Nobutaka Mukumoto[1], Mitsuhiro Nakamura*[1], Akira Sawada[1,2], Yasunobu Suzuki[3], Kunio Takahashi[1,3], Yuki Miyabe[1], Shuji Kaneko[1,3], Takashi Mizowaki[1], Masaki Kokubo[4,5], and Masahiro Hiraoka[1]

[1]Department of Radiation Oncology and Image-applied Therapy, Graduate School of Medicine, Kyoto University, Kyoto 606-8507, Japan

[2]Department of Radiological Technology, Faculty of Medical Science, Kyoto College of Medical Science, Nantan 622-0041, Japan

[3]Advanced Mechanical Systems Department, Mitsubishi Heavy Industries Ltd., Hiroshima 733-8553, Japan

[4]Department of Radiation Oncology, Kobe City Medical Center General Hospital, Kobe 650-0047, Japan

[5]Division of Radiation Oncology, Institute of Biomedical Research and Innovation, Kobe 650-0047, Japan

***Corresponding author**: Mitsuhiro Nakamura, Ph.D., Graduate School of Medicine, Kyoto University, 54 Kawahara-cho, Shogoin, Sakyo-ku, Kyoto, 606-8507, Japan.

Tel.: +81-75-751-3762; Fax: +81-75-771-9749; E-mail: m_nkmr@kuhp.kyoto-u.ac.jp

Running title: Accuracy verification of IR Tracking with the Vero4DRT.

Conflicts of interest: This research was in part sponsored by Mitsubishi Heavy Industries, Ltd., Japan. Takashi Mizowaki, Masaki Kokubo, and Masahiro Hiraoka have consultancy agreements with Mitsubishi Heavy Industries, Ltd., Japan.

Meeting presentation: This research was presented orally, in part, at the American Association of Physicists in Medicine (AAPM) 54th Annual Meeting in Charlotte, July 29 to August 2, 2012.

Abstract

Purpose: To verify the accuracy of an infrared (IR) marker-based dynamic tumor-tracking irradiation system (IR Tracking) using the gimbaled x-ray head of the Vero4DRT (MHI-TM2000).

Methods and Materials: The gimbaled 6-MV C-band x-ray head of the Vero4DRT can swing along the pan-and-tilt direction to track a moving target. During beam delivery, the Vero4DRT predicts the future three-dimensional (3D) target position in real time using a correlation model (4D model) between the target and IR marker motion, and then continuously transfers the corresponding tracking orientation to the gimbaled x-ray head. The 4D-modeling error (E_{4DM}) and the positional tracking error (E_P) were defined as the difference between the predicted and measured positions of the target in 4D modeling and as the difference between the tracked and measured positions of the target during irradiation, respectively. For the clinical application of IR Tracking, we assessed the relationship between E_{4DM} and E_P for three 1D sinusoidal (peak-to-peak amplitude [A]: 20-40 mm, breathing period [T]: 2-4 s), five 1D phase-shifted sinusoidal (A: 20 mm, T: 4 s, phase shift [τ]: 0.2-2 s), and six 3D patient respiratory patterns.

Results: The difference between the 95th percentile of the absolute E_P (E_P^{95}) and the mean (μ) + two standard deviations (SD) of absolute E_{4DM} ($E_{4DM}^{\mu+2SD}$) was within ±1 mm for all motion patterns. As the absolute correlation between the target and IR marker motions decreased from 1.0 to 0.1 for the 1D phase-shifted sinusoidal patterns, the $E_{4DM}^{\mu+2SD}$ and E_P^{95} increased linearly, from 0.4 to 3.0 mm (R = -0.98) and from 0.5 to 2.2 mm (R = -0.95), respectively. There was a strong positive correlation between $E_{4DM}^{\mu+2SD}$ and E_P^{95} in each direction [(lateral, craniocaudal, anteroposterior) = (0.99, 0.98, 1.00)], even for the 3D respiratory patterns; thus, E_P^{95} was readily estimated from $E_{4DM}^{\mu+2SD}$.

Conclusions: Positional tracking errors correlated strongly with 4D-modeling errors in IR

Tracking. Thus, the accuracy of the 4D model must be verified before treatment, and margins are required to compensate for the 4D-modeling error.

Key words: Four-dimensional image-guided radiotherapy, dynamic tumor-tracking irradiation, intrafractional respiratory motion, gimbaled x-ray head, tracking accuracy.

I. INTRODUCTION

The International Commission on Radiation Units and Measurements (ICRU) recommends that the planning target volume (PTV) includes margins around a clinical target volume (CTV) to account for patient motion, tumor motion, and deformation due to respiration and uncertainties in beam placement.[1,2] Particularly for thoracic and abdominal tumors, respiration is an important factor causing uncertainty during beam delivery. Several techniques, including respiratory gating, breath-holding, and dynamic tumor tracking (DTT), have been proposed to reduce the uncertainties caused by respiratory motion.[3] Among these techniques, DTT can minimize the internal uncertainties without a prolonged treatment time or the burden of breath-holding for patients. There are two approaches to DTT: direct and indirect methods.[3,4] While direct methods detect the target itself, indirect methods assess some surrogate quantity and deduce localization information based on the surrogate.

We have developed a novel four-dimensional (4D) image-guided radiotherapy system with a DTT function: the Vero4DRT (MHI-TM2000; Mitsubishi Heavy Industries, Ltd., Japan, and BrainLAB, Feldkirchen, Germany).[5-11] Figure 1 shows a schematic diagram of the Vero4DRT. The Vero4DRT has several unique components that facilitate DTT irradiation: (1) a compact C-band 6-MV x-ray head with a gimbal mechanism, mounted on an O-ring gantry. The gimbaled x-ray head can rotate in both the pan (horizontal to the O-ring) and tilt (vertical to the O-ring) directions, (2) a gantry-mounted orthogonal kV x-ray imaging subsystem, consisting of two sets of x-ray tubes and flat-panel detectors, with a spatial resolution of 0.2 mm at the isocenter level, and (3) an extended version of the ExacTRAC system for the DTT function (BrainLAB)[12,13] with an infrared (IR) camera mounted on the ceiling of the treatment room.

The Vero4DRT is capable of direct and indirect DTT approaches. One is an x-ray image-based direct DTT approach (X-ray Tracking).[9,10] A moving tumor is tracked in real time

by either direct monitoring of the tumor itself or fiducial markers, using the kV x-ray imaging subsystem. However, the x-ray monitoring interval and image processing time delay cause prediction errors.[10] Furthermore, continuous x-ray monitoring may result in two potential health hazards: deterministic and stochastic risks associated with the increased radiation dose delivered by the kV x-ray imaging subsystem.[14-17] The other is an IR marker-based indirect DTT approach (IR Tracking), which is available clinically. An advantage of IR Tracking is a substantial reduction in imaging dose, compared with that of X-ray Tracking. During beam delivery, the Vero4DRT monitors the displacement of the IR markers on the abdominal wall continuously via the IR camera of the ExacTRAC system, and then tracks target motion using a correlation model (4D model) between the target and IR marker motions, as described in Section II. A.

A key issue in indirect DTT is the accuracy of the model predicting the internal target position based on the surrogate measurements.[3,4] Several investigators have shown that the Synchrony Respiratory Tracking System, part of the Cyberknife indirect DTT system (Accuracy Inc., Sunnyvale, CA), was able to follow a moving tumor with high accuracy.[18-22] Depuydt *et al*. verified the positional tracking accuracy of IR Tracking only under conditions of a perfect correlation between the target and IR marker motions using a prototype of the Vero4DRT;[13] however, no dosimetric verification was performed. According to the report of the American Association of Physicists in Medicine Task Group 76, phase shifts between the internal tumor and external surrogate motion of > 1 s were observed in patients with lung cancer.[3] The accuracy of a 4D model is unknown in the presence of such a phase shift. Additionally, tracking accuracy – based on the respiratory tumor and abdominal wall motions of real patients – should be verified before the clinical use of IR Tracking. Thus, in the present study, we verified the dosimetric and positional accuracy of IR Tracking.

II. MATERIALS AND METHODS

II. A. The 4D model for IR Tracking with the Vero4DRT

Figure 2 shows a schematic diagram of IR Tracking. Before irradiation, IR marker displacements on the abdominal wall and the implanted fiducial markers' motion are monitored to create a 4D model for 20-40 s using the IR camera of the ExacTRAC system every 16.7 ms and the orthogonal kV x-ray imaging subsystem every 80 ms, using a stereovision technique. After monitoring, two target positions are determined: the detected target position and the predicted target position. The detected target position is indicated by the centroid of the polyhedron, composed from the implanted fiducial markers. The predicted target position is calculated from the 4D model, expressed by a quadratic equation involving two variables, the position and velocity of the IR markers. In the 4D-modeling phase, the peak-to-peak amplitude of the detected target motion (A) and the mean (μ) and standard deviation (SD) of the absolute difference between the detected and predicted target positions are automatically calculated along each axis (Fig. 2). During beam delivery, the 3D target position is calculated from the displacements of the IR markers using the 4D model, and then the corresponding tracking orientation is transferred continuously to the gimbaled x-ray head. The predicted target position can also be monitored visually in real time at a minimum interval of 1 s on intra-fractional fluoroscopic images.

II. B. Dosimetric and positional verification of IR Tracking

For the clinical application of IR Tracking, the following verifications were performed:

(1) Dosimetric and positional verification of 1D sinusoidal patterns with perfect correlation between the target and IR marker motions, using a motor-driven base.

(2) Positional verification of 1D sinusoidal patterns with miscorrelation between the target and IR marker motions, using a dynamic anthropomorphic thorax phantom.

(3) Positional verification of 3D target and 1D surrogate motions, based on the patient's respiration, using a four-axis moving phantom.

II. B. 1. Dosimetric and positional verification of IR Tracking for 1D sinusoidal patterns

Figure 3(a) shows a photograph of the experimental system for the dosimetric and positional verification of IR Tracking. The IR markers were moved synchronously with the 1D motor-driven base (QUASAR, Modus Medical Devices Inc., London, ON, Canada) in the anteroposterior (AP) direction.

Dosimetric verification was performed using EDR2 film (Kodak, Rochester, NY, USA), placed at a depth of 100 mm (1000 mm source-to-isocenter distance) in water-equivalent phantoms on the motor-driven base. Four pinholes were made on the film to identify the isocenter. The EDR2 film (Kodak, Rochester, NY, USA) was irradiated with a field size of 50×50 mm^2 under stationary, tracking, and non-tracking states for 1D sinusoidal patterns (A: 20-40 mm, breathing period [T]: 2-4 s) in the craniocaudal (CC) direction. In total, seven irradiated films were scanned in the same orientation (ES-10000G; Epson Corp., Nagano, Japan) with a resolution of 150 dpi in 16-bit grayscale with a 12-h postexposure period. All films were analyzed using commercially available radiation dosimetry software (DD system, ver. 9.4; R'Tech Inc., Tokyo, Japan). Differences in the width of the 95% dose profile between stationary and moving conditions (E_D^{95}) were calculated.

Additionally, positional verification was performed using a laser displacement gauge (IL-300; Keyence Corp., Osaka, Japan), with a positional accuracy of 0.05 mm. The laser displacement gauge was used for independent validation of IR Tracking and was not part of the Vero4DRT IR Tracking system. In the experiment, the target position was measured with the

laser displacement gauge every 10 ms for independent validation, and the laser displacement signals were sent to a system controller for synchronization of the data recording. The Vero4DRT records IR Tracking logs into the system controller every 5 ms. Based on the recorded tracking orientation of the gimbaled x-ray head, the tracked position of the target on the isocenter plane was calculated as follows:

$$y_t = -960\tan(\theta_T),$$

where y_t is the tracked position of the target in the CC direction, θ_T is the tilt angle of the gimbaled x-ray head, and 960 mm is the distance from the rotation center of the gimbals to the isocenter. The positional tracking error (E_P) was defined as $E_P = y_t - y_{ml}$, where y_{ml} is the phantom position in the CC direction, measured with the laser displacement gauge. The 95th percentile of the E_P (E_P^{95}) was then calculated.

II. B. 2. Positional verification of IR Tracking for 1D phase-shifted sinusoidal patterns

Figure 3(b) shows a photograph of the experimental system for the positional verification of IR Tracking for the 1D phase-shifted sinusoidal patterns (A: 20 mm, T: 4 s, phase shift [τ]: 0.2-2 s):

$$y_p(t) = 0.5A\sin(\omega t/T),$$

$$z_s(t) = 0.5A\sin\{\omega(t-\tau)/T\},$$

where $y_p(t)$ is the phantom position in the CC direction and $z_s(t)$ is the displacement of the IR markers in the AP direction. Positional accuracy was evaluated using the dynamic anthropomorphic thorax phantom (CIRS Inc., Norfolk, VA) with a high precision (0.1 mm) laser displacement gauge. E_P^{95} was estimated as described in Section II. B. 1.

II. B. 3. Positional verification of IR Tracking for 3D respiratory patterns

Figure 3(c) shows a photograph of the experimental system for the positional

verification of IR Tracking with the 3D respiratory patterns acquired from six lung cancer patients. IR markers for measurement using Polaris Spectra (Northern Digital Inc., Waterloo, Ontario, Canada) and fiducial markers for measurement using the gantry-mounted orthogonal kV x-ray imaging subsystem were attached to the surface of a cubic phantom. The Polaris Spectra was used for independent validation of IR Tracking and was not part of the Vero4DRT IR Tracking system. Then, the cubic phantom was placed firmly on the 3D-driven base of a four-axis moving phantom, which moved three-dimensionally, based on the acquired internal target motions. Other IR markers for IR Tracking were also placed on the 1D driven base of the four-axis moving phantom, which moved based on the acquired IR marker motions in the AP direction only. The four-axis moving phantom was able to reproduce patient respiratory motions with high precision (0.1 mm).[23] The positions of the IR markers for measurement ($P_{mP}[x_{mP}, y_{mP}, z_{mP}]$) and fiducial markers for measurement ($P_{mX}[x_{mX}, y_{mX}, z_{mX}]$) were measured with the Polaris Spectra, with a measurement accuracy of 0.3 mm, every 16.7 ms, and by the gantry-mounted orthogonal kV x-ray imaging subsystem every 1 s, respectively. In the present study, these positional data were recorded synchronously, based on the exposer signal of the orthogonal kV x-ray imaging subsystem.

First, the detection accuracy of the gantry-mounted orthogonal kV x-ray imaging subsystem was evaluated in the stationary condition using the treatment couch, with a positional accuracy of 0.01 mm. Second, in total, 742 comparisons between P_{mP} and P_{mX} were made to evaluate the detection accuracy of the gantry-mounted orthogonal kV x-ray imaging subsystem in the moving condition using the Polaris Spectra and the four-axis moving phantom.

To investigate the tracking accuracy in each direction, positional verification was performed at gantry angles of 0° and 90°. Based on the recorded tracking orientation of the gimbaled x-ray head, the tracked position of the target was estimated on the perpendicular

plane to the home gimbal-axis at the measured target position.[10] At a gantry angle of 0°, the tracked position of the target was calculated as follows:

$$x_t = (960 - z_{mX}) \tan(\theta_P),$$

$$y_t = -(960 - z_{mX}) \tan(\theta_T),$$

where x_t is the tracked position of the target in the lateral (LR) direction, θ_P is the pan angle of the gimbaled x-ray head, y_t is the tracked position of the target in the CC direction, and θ_T is the tilt angle of the gimbaled x-ray head. At a gantry angle of 0°, the tracked position of the target at the gantry angle of 90° was calculated as follows:

$$y_t = -(960 - x_{mX}) \tan(\theta_T),$$

$$z_t = (960 - x_{mX}) \tan(\theta_P),$$

where z_t is the tracked position of the target in the AP direction. The E_P was defined as follows:

$$E_P = \begin{pmatrix} x_t \\ y_t \\ z_t \end{pmatrix} - \begin{pmatrix} x_{mX} \\ y_{mX} \\ z_{mX} \end{pmatrix}.$$

E_P^{95} was estimated as described in Sections II. B. 1. and II. B. 2.

III. RESULTS AND DISCUSSION

III. A. Dosimetric and positional verification of IR Tracking for 1D sinusoidal patterns

Figure 4(a) shows dose profiles of a 50×50-mm^2 field under stationary, tracking, and non-tracking states for the sinusoidal patterns with (A, T) = (40 mm, 2 s). The blurred effect, due to phantom motion, was reduced substantially by IR Tracking, comparable with previous results.[9] Figure 4(b) shows variations in the tracked and measured positions of the target for the sinusoidal patterns with (A, T) = (40 mm, 2 s) in the CC direction. Even for the severe motion

pattern, the gimbaled x-ray head tracked the target in real time with high accuracy.

Table I summarizes μ + 2SD of the absolute 4D-modeling error ($E_{4DM}^{\mu+2SD}$), E_D^{95}, and E_P^{95} of 1D sinusoidal patterns. $E_{4DM}^{\mu+2SD}$ was calculated from the μ and SD displayed on the screen of the Vero4DRT in the 4D-modeling phase. Under conditions of perfect correlation between the target and IR marker motions, $E_{4DM}^{\mu+2SD}$ ranged from 1.4 to 1.9 mm. E_D^{95} ranged from 11.2 to 29.6 mm in the non-tracking state; however, these values were reduced by 0.0 to 1.2 mm in the tracking state. IR Tracking reduced blurring dramatically and produced a dose-profile slope similar to that of the stationary state. Additionally, the measured and tracked positions of the target were consistent with each other. E_P^{95} ranged from 1.3 to 1.8 mm in the tracking state and from 9.9 to 19.9 mm in the non-tracking state, and E_P^{95} in the tracking state was similar to $E_{4DM}^{\mu+2SD}$. As shown in Table I, E_D^{95} was much smaller than twice E_P^{95} because the randomized dose errors were partially cancelled out at the field edge; thus, assessment of E_P^{95} represents an alternative safety indicator in terms of determining whether the internal margin for IR Tracking is adequate in clinical practice.

III. B. Positional verification of IR Tracking for 1D phase-shifted sinusoidal patterns

Table II summarizes the absolute correlation coefficient between the target and IR marker motions ($|R_{IR}^{target}|$), $E_{4DM}^{\mu+2SD}$, and E_P^{95} for phase-shifted sinusoidal patterns. As $|R_{IR}^{target}|$ became small, $E_{4DM}^{\mu+2SD}$ and E_P^{95} increased linearly, from 0.4 to 3.0 mm (R = -0.98) and from 0.5 to 2.2 mm (R = -0.95), respectively. A strong positive correlation was also found between $E_{4DM}^{\mu+2SD}$ and E_P^{95} (R = 0.99). In the 4D-modeling process, the 4D model was created to minimize residual errors between the predicted and detected target positions. Thus, the relationship between E_P^{95} and E_D^{95} will be almost equivalent even in the presence of a phase shift.

III. C. Positional verification of IR Tracking for 3D respiratory patterns

The root mean squares (RMSs) of the detection accuracy of the gantry-mounted orthogonal kV x-ray imaging subsystem under the stationary condition were 0.07, 0.04, and 0.03 mm in the LR, CC, and AP directions, respectively. The RMSs of the detection accuracy of the gantry-mounted orthogonal kV x-ray imaging subsystem under the moving condition were 0.14, 0.39, and 0.15 mm in the LR, CC, and AP directions, respectively. These results show that the gantry-mounted orthogonal kV x-ray imaging subsystem of the Vero4DRT had high detection accuracy, even for moving targets.

Figure 5 shows variations in the target position along the CC direction for the respiratory pattern of the first patient who underwent IR Tracking (Patient No. 3). E_P^{95} was 1.6 mm for this patient.

Table III summarizes $E_{4DM}^{\mu+2SD}$ and E_P^{95} for respiratory patterns. A strong negative correlation between $|R_{IR}^{target}|$ and $E_{4DM}^{\mu+2SD}/A$ was observed in each direction [(LR, CC, AP) = (-0.88, -0.90, -0.92)]. A strong positive correlation was also found between $E_{4DM}^{\mu+2SD}$ and E_P^{95} in each direction [(LR, CC, AP) = (0.99, 0.98, 1.00)]; thus, E_P^{95} was readily estimated from $E_{4DM}^{\mu+2SD}$. Figure 6 shows accumulated probability histograms (a) as a function of the positional tracking errors and (b) as a function of the tracking efficiency, defined as the $2E_P^{95}/A$, in each direction at gantry angles of 0° and 90°. The positional tracking errors were larger in the CC direction than in the other directions [Fig. 6(a)]. However, the tracking efficiencies were the highest in the CC direction [Fig. 6(b)]. Lower tracking efficiencies in other directions than in the CC direction were caused by the small $|R_{IR}^{target}|$ (Table III). Additionally, tracking accuracy was not degraded by gantry rotation, even at an angle of 90°.

Pepin *et al.* suggested that a dry-run treatment session prior to treatment planning is required to determine patient-specific margins covering positional tracking error during the treatment when performing DTT with the Synchrony Respiratory Tracking System.[22] The

present study revealed that positional tracking errors were near-identical to 4D-modeling errors, derived from miscorrelation between the target and abdominal wall motions, such as the phase shift or irregular respiration. Thus, users of the Vero4DRT should evaluate the accuracy of the 4D model in a dry-run treatment session, and the following should then be discussed, based on the acquired 4D-modeling accuracy: (1) adding margins to compensate for 4D-modeling errors and (2) conducting respiratory coaching to minimize the phase shift.[24]

The correlation between tumor and surrogate motion is known to change from treatment planning to treatment delivery.[3,25,26] The change in correlation may cause additional tracking errors in IR Tracking; thus, additional margins to compensate for these uncertainties are required, and confirmation of whether the 4D-modeling errors for each fraction are within the margin derived from 4D-modeling errors at treatment planning is recommended. Additionally, Malinowski *et al*. reported that an extended treatment time can lead to miscorrelation between the external surrogate and internal tumor motion, due to baseline drift.[27] During irradiation, we can estimate visually the tracking errors in real time from the implanted fiducial markers – or the tumor itself – on the intra-fractional fluoroscopic images. When these positions deviate systematically from those predicted, due to baseline drift or changes in respiration, remodeling of the 4D model during a treatment fraction is required to perform IR Tracking safely.

IV. CONCLUSIONS

We verified the dosimetric and positional accuracy of IR Tracking and confirmed its feasibility in clinical practice. IR Tracking reduced substantially motion-induced marginal blurring in the dose distribution. Additionally, positional tracking errors correlated strongly with 4D-modeling errors, which resulted from miscorrelations between target and IR marker motions. Thus, the accuracy of the 4D model must be verified before treatment, and margins

are required to compensate for 4D-modeling errors.

ACKNOWLEDGMENTS

The authors express their appreciation to the entire technical staff at MHI for providing detailed information on the gimbaled x-ray head-tracking system and acquiring the experimental data. This research was supported by the Japan Society for the Promotion of Science (JSPS) through its “Funding Program for World-Leading Innovative R&D on Science and Technology (FIRST Program)” and a Grant-in-Aid for Scientific Research from the Association for Nuclear Technology in Medicine.

REFERENCES

1. "Prescribing, recording and reporting photon beam therapy." ICRU Report 50, International Commission on Radiation Units and Measurements, Bethesda, MD (1993).
2. "Prescribing, recording and reporting photon beam therapy." ICRU Report 62 (Supplement to ICRU Report 50), International Commission on Radiation Units and Measurements, Bethesda, MD (1999).
3. P. J. Keall, G. S. Mageras, J. M. Balter, R. S. Emery, K. M. Forster, S. B. Jiang, J. M. Kapatoes, D. A. Low, M. J. Murphy, B. R. Murray, C. R. Ramsey, M. B. Van Herk, S. S. Vedam, J. W. Wong, and E. Yorke, "The management of respiratory motion in radiation oncology report of AAPM task group 76," Med. Phys. **33**, 3874–3900 (2006).
4. S. Dieterich, K. Cleary, W. D'Souza, M. Murphy, K. H. Wong, and P. J. Keall, "Locating and targeting moving tumors with radiation beams," Med. Phys. **35**, 5684–5694 (2008).
5. Y. Kamino, K. Takayama, M. Kokubo, Y. Narita, E. Hirai, N. Kawada, T. Mizowaki, Y. Nagata, T. Nishidai, and M. Hiraoka, "Development of a four-dimensional image-guided radiotherapy system with a gimbaled X-ray head," Int. J. Radiat. Oncol. Biol. Phys. **66**, 271–278 (2006).
6. Y. Kamino, S. Miura, M. Kokubo, I. Yamashita, E. Hirai, M. Hiraoka, and J. Ishikawa, "Development of an ultrasmall C-band linear accelerator guide for a four-dimensional image-guided radiotherapy system with a gimbaled x-ray head," Med. Phys. **34**, 1797–1808 (2007).
7. A. Sawada, S. Kaneko, K. Takayama, K. Nagano, Y. Miyabe, M. Nakamura, Y. Narita, K. Takahashi, M. Kokubo, T. Mizowaki, and M. Hiraoka, "Daily verification of isocenter alignment for a new image guided radiotherapy system, MHI-TM2000," Med. Phys. **36**, 2586–2587 (2009).
8. M. Nakamura, A. Sawada, Y. Ishihara, K. Takayama, T. Mizowaki, S. Kaneko, M.

Yamashita, H. Tanabe, M. Kokubo, and M. Hiraoka, "Dosimetric characterization of a multileaf collimator for a new four-dimensional image-guided radiotherapy system with a gimbaled x-ray head, MHI-TM2000," Med. Phys. **37**, 4684–4691 (2010).

9. K. Takayama, T. Mizowaki, M. Kokubo, N. Kawada, H. Nakayama, Y. Narita, K. Nagano, Y. Kamino, and M. Hiraoka, "Initial validations for pursuing irradiation using a gimbals tracking system," Radiother. Oncol. **93**, 45–49 (2009).
10. N. Mukumoto, M. Nakamura, A. Sawada, K. Takahashi, Y. Miyabe, K. Takayama, T. Mizowaki, M. Kokubo, and M. Hiraoka, "Positional accuracy of novel x-ray-image-based dynamic tumor-tracking irradiation using a gimbaled MV x-ray head of a Vero4DRT (MHI-TM2000)," Med. Phys. **39**, 6287–6296 (2012).
11. Y. Miyabe, A. Sawada, K. Takayama, S. Kaneko, T. Mizowaki, M. Kokubo, and M. Hiraoka, "Positioning accuracy of a new image-guided radiotherapy system," Med. Phys. **38**, 2535–2541 (2011).
12. Weiss E, Vorwerk H, Richter S, and C. F. Hess, "Interfractional and intrafractional accuracy during radiotherapy of gynecologic carcinomas: a comprehensive evaluation using the ExacTrac system," Int. J. Radiat. Oncol. Biol. Phys. **56**, 69–79 (2003).
13. T. Depuydt, D. Verellen, O. Haas, T. Gevaert, N. Linthout, M. Duchateau, K. Tournel, T. Reynders, K. Leysen, M. Hoogeman, G. Storme, and M. De Ridder, "Geometric accuracy of a novel gimbals based radiation therapy tumor tracking system," Radiother. Oncol. **98**, 365–372 (2011).
14. K. Takayama, N. Kawada, K. Nagano, Y. Sato, Y. Matsuo, T. Mizowaki, M. Kokubo, H. Nakayama, Y. Narita, and M. Hiraoka, "Imaging dose on a dual on-board kV x-ray imaging system in MHI-TM2000," Int. J. Radiat. Oncol. Biol. Phys. **72**, S655–S656 (2008).
15. M. J. Murphy, J. Balter, S. Balter, J. A. BenComo, I. J. Das, S. B. Jiang, C. M. Ma, G. H.

Olivera, R. F. Rodebaugh, K. J. Ruchala, H. Shirato, and F. F. Yin, "The management of imaging dose during image-guided radiotherapy: report of the AAPM Task Group 75," Med. Phys. **34**, 4041–4063 (2007).

16. M. K. Islam, T. G. Purdie, B. D. Norrlinger, H. Alasti, D. J. Moseley, M. B. Sharpe, J. H. Siewerdsen, and D. A. Jaffray, "Patient dose from kilovoltage cone beam computed tomography imaging in radiation therapy," Med. Phys. **33**, 1573–1582 (2006).
17. C. L. Perkins, T. Fox, E. Elder, D. A. Kooby, C. A. Staley, and J. Landry, "Image-guided radiation therapy (IGRT) in gastrointestinal tumors," JOP. **7**, 372–381 (2006).
18. A. Schweikard, H. Shiomi, and J. Adler, "Respiration tracking in radiosurgery," Med. Phys. **31**, 2738–2741 (2004).
19. Y. Seppenwoolde, R. I. Berbeco, S. Nishioka, H. Shirato, and B. Heijmen, "Accuracy of tumor motion compensation algorithm from a robotic respiratory tracking system: a simulation study," Med. Phys. **34**, 2774–2784 (2007).
20. E. Nioutsikou, Y. Seppenwoolde, J. R. Symonds-Tayler, B. Heijmen, P. Evans, and S. Webb, "Dosimetric investigation of lung tumor motion compensation with a robotic respiratory tracking system: an experimental study," Med. Phys. **35**, 1232–1240 (2008).
21. M. Hoogeman, J. B. Prévost, J. Nuyttens, J. Pöll, P. Levendag, and B. Heijmen, "Clinical accuracy of the respiratory tumor tracking system of the cyberknife: assessment by analysis of log files," Int. J. Radiat. Oncol. Biol. Phys. **74**, 297–303 (2009).
22. E. W. Pepin, H. Wu, Y. Zhang, and B. Lord, "Correlation and prediction uncertainties in the cyberknife synchrony respiratory tracking system," Med. Phys. **38**, 4036-4044 (2011).
23. H. Nakayama, T. Mizowaki, Y. Narita, and M. Hiraoka, "Development of a three-dimensionally movable phantom system for dosimetric verifications," Med. Phys. **35**, 1643–1650 (2008).

24. M. Nakamura, Y. Narita, Y. Matsuo, M. Narabayashi, M. Nakata, A. Sawada, T. Mizowaki, Y. Nagata, and M. Hiraoka, “ Effect of audio coaching on correlation of abdominal displacement with lung tumor motion,” Int. J. Radiat. Oncol. Biol. Phys. **75**, 558-563 (2009).

25. K. J. Redmond, D. Y. Song, J. L. Fox, J. Zhou, C. N. Rosenzweig, and E. Ford, “Respiratory motion changes of lung tumors over the course of radiation therapy based on respiration-correlated four-dimensional computed tomography scans,” Int. J. Radiat. Oncol. Biol. Phys. **75**, 1605–1612 (2009).

26. S. S. Korreman, T. Juhler-Nøttrup, and A. L. Boyer, “Respiratory gated beam delivery cannot facilitate margin reduction, unless combined with respiratory correlated image guidance,” Radiother. Oncol. **98**, 365–372 (2008).

27. K. Malinowski, T. J. McAvoy, R. George, S. Dietrich, and W. D. D’Souza, “Incidence of changes in respiration-induced tumor motion and its relationship with respiratory surrogates during individual treatment fractions,” Int. J. Radiat. Oncol. Biol. Phys. **82**, 1665–1673 (2012).

FIGURE LEGENDS

Figure 1. Schematic diagram of the Vero4DRT.

Figure 2. Schematic diagram of infrared (IR) marker-based dynamic tumor-tracking irradiation (IR Tracking). In the 4D-modeling phase, the mean and standard deviation of the absolute 4D-modeling error, as well as the peak-to-peak amplitude of the target motion, are shown on the screen of the Vero4DRT. The right four groups of waves, from top to bottom, show variations in the IR markers' positions in the anteroposterior (AP) direction and the target positions in the lateral (LR), craniocaudal (CC), and AP directions, respectively. In the graphs of the target position, dark-colored waves show the detected target position and light-colored waves show the predicted target position. During beam delivery, the future 3D target position is calculated from the displacements of the IR markers using the 4D model, and then the corresponding tracking orientation is transferred continuously to the gimbaled x-ray head.

Figure 3. Photograph of the experimental system for (a) dosimetric and positional verification of infrared (IR) marker-based dynamic tumor-tracking (IR Tracking) of 1D sinusoidal patterns, (b) positional verification of 1D phase-shifted sinusoidal patterns, and (c) positional verification of the 3D respiratory patterns of six patients with lung cancer.

Figure 4. (a) Dose profile of a 50×50 mm^2 field under stationary, tracking, and non-tracking states and (b) variations in the tracked and measured positions of the target for the sinusoidal pattern with a peak-to-peak amplitude of 40 mm and breathing period of 2 s.

Figure 5. Variations in the target position along the craniocaudal (CC) direction for the

respiratory pattern of the first patient who underwent IR Tracking (Patient No. 3). Square symbols indicate the detected positions of the target, solid lines with round symbols indicate the tracked positions of the target, and dotted lines show positional tracking errors.

440

Figure 6. Accumulated probability histogram (a) as a function of the 95th percentile of the positional tracking error (E_P^{95}) and (b) as a function of the tracking efficiency, defined as the ratio of twice the 95th percentile of the positional tracking error (E_P^{95}) to the peak-to-peak amplitude (A), in the lateral (LR), craniocaudal (CC), and anteroposterior (AP) directions

445 under gantry angles of 0° (G0deg) and 90° (G90deg).

TABLES

TABLE I. $E_{4DM}^{\mu+2SD}$, E_D^{95}, and E_P^{95} under non-tracking and tracking states for sinusoidal patterns.

Case	A [mm]	T [s]	$E_{4DM}^{\mu+2SD}$ [mm]	Non-tracking		Tracking	
				E_D^{95} [mm]	E_P^{95} [mm]	E_D^{95} [mm]	E_P^{95} [mm]
1	40	2	1.8	29.6	19.9	1.2	1.8
2	40	4	1.9	29.4	19.9	0.2	1.8
3	20	2	1.4	11.2	9.9	0.0	1.3

Abbreviations: μ = mean; SD = standard deviation; $E_{4DM}^{\mu+2SD}$ = μ+2SD of the absolute 4D-modeling error; E_D^{95} = differences in the width of the 95% dose profile between stationary and moving conditions; E_P^{95} = 95th percentile of the positional tracking error; A = peak-to-peak amplitude; T = breathing period.

TABLE II. $|R_{IR}^{target}|$, $E_{4DM}^{\mu+2SD}$, and E_P^{95} of phase-shifted sinusoidal patterns with a peak-to-peak amplitude of 20 mm and breathing period of 4 s.

Case	τ [s]	$\lvert R_{IR}^{target} \rvert$	$E_{4DM}^{\mu+2SD}$ [mm]	E_P^{95} [mm]
1	0.0	1.00	0.4	0.6
2	0.2	0.95	0.6	0.7
3	0.4	0.82	1.4	1.4
4	1.0	0.10	3.0	2.2
5	2.0	1.00	0.4	0.5

Abbreviations: $|R_{IR}^{target}|$ = absolute correlation coefficient between target and IR marker motions; μ = mean; SD = standard deviation; $E_{4DM}^{\mu+2SD}$ = μ+2SD of the absolute 4D-modeling error; E_P^{95} = 95th percentile of the positional tracking error; τ = phase shift.

460 **TABLE III**. $|R_{IR}^{target}|$, $E_{4DM}^{\mu+2SD}$ and E_P^{95} of respiratory patterns.

Patient no.	A [mm]			T [s]	$\lvert R_{IR}^{target} \rvert$			$E_{4DM}^{\mu+2SD}$ [mm]			E_P^{95} [mm]		
	LR	CC	AP		LR	CC	AP	LR	CC	AP	LR	CC	AP
1	2.4	13.9	7.5	3.6	0.78	0.91	0.01	0.6	3.0	3.2	0.7	2.9	2.6
2	2.0	35.2	5.6	5.5	0.41	0.99	0.93	1.0	3.3	1.4	0.9	3.6	1.2
3	1.7	11.9	1.5	3.4	0.98	0.98	0.26	0.2	1.3	0.5	0.2	1.5	0.6
4	4.2	17.0	3.4	3.5	0.92	0.99	0.93	1.2	2.5	0.4	1.2	2.6	0.5
5	1.7	21.2	3.3	3.4	0.97	0.98	0.92	0.3	2.4	0.5	0.3	2.4	0.6
6	0.7	10.7	2.6	3.1	0.17	0.99	0.60	0.3	1.0	0.7	0.3	1.0	0.8

Abbreviations: $|R_{IR}^{target}|$ = absolute correlation coefficient between target and IR marker motions; μ = mean; SD = standard deviation; $E_{4DM}^{\mu+2SD}$ = μ+2SD of the absolute 4D-modeling error; E_P^{95} = 95th percentiles of the positional tracking error; A = peak-to-peak amplitude; T = breathing period; LR = lateral direction; CC = craniocaudal direction; AP = anteroposterior direction.

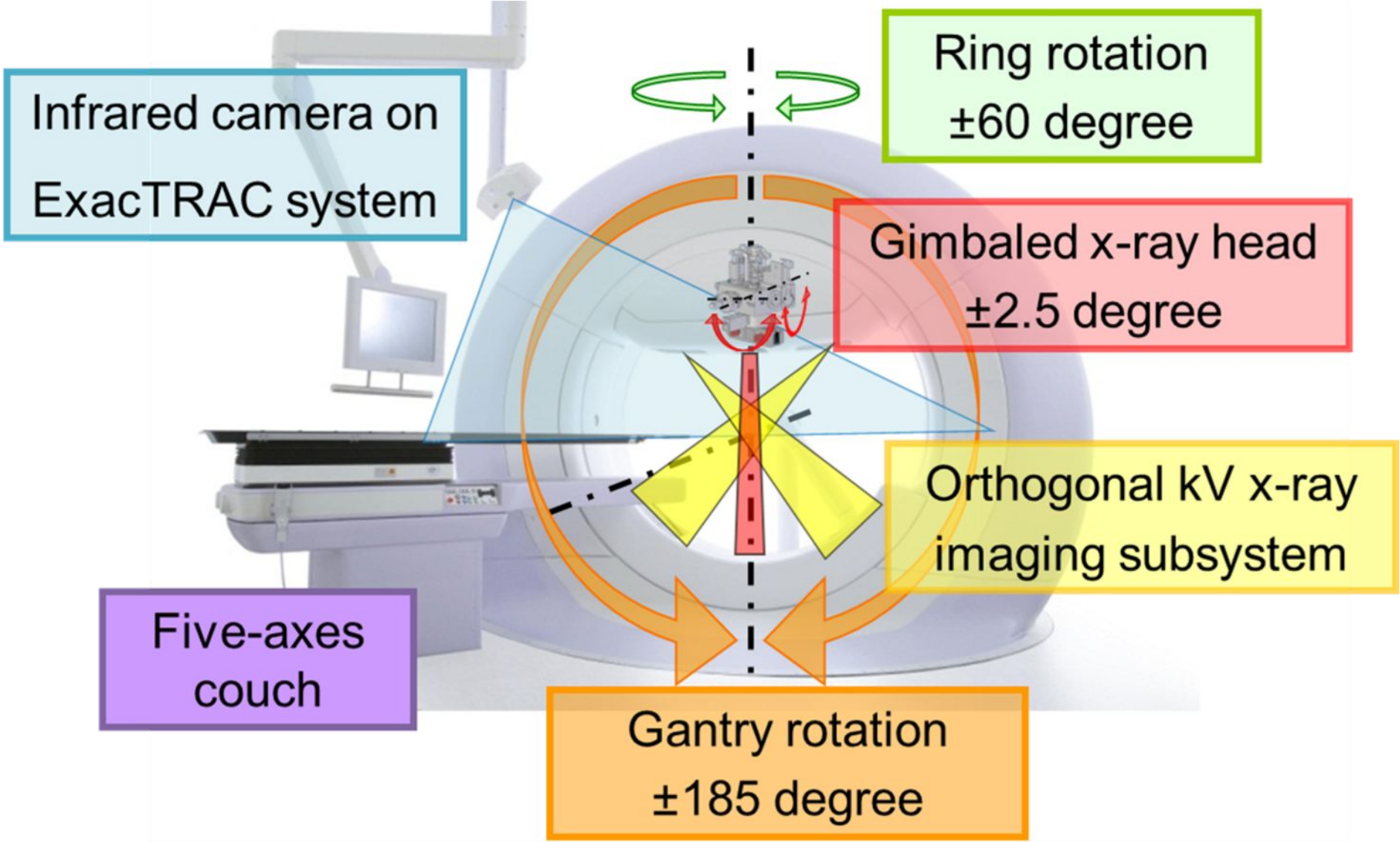
Infrared camera on ExacTRAC system
Ring rotation ±60 degree
Gimbaled x-ray head ±2.5 degree
Orthogonal kV x-ray imaging subsystem
Five-axes couch
Gantry rotation ±185 degree

4D-modeling phase

Orthogonal kV x-ray tube

IR camera on ExacTRAC system

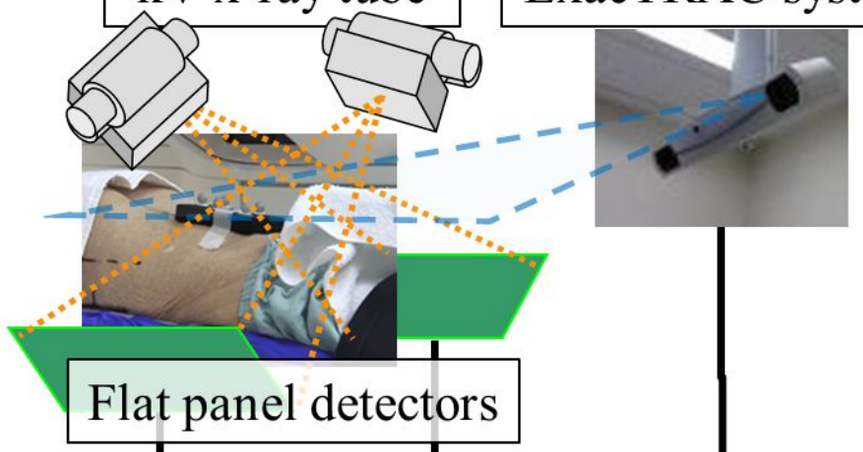

Flat panel detectors

Orthogonal fluoro-scopic images

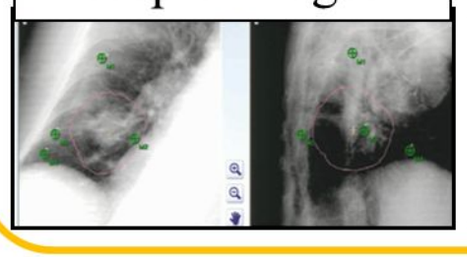

Displacements of IR markers

Screen of the Vero4DRT for the 4D-modeling phase

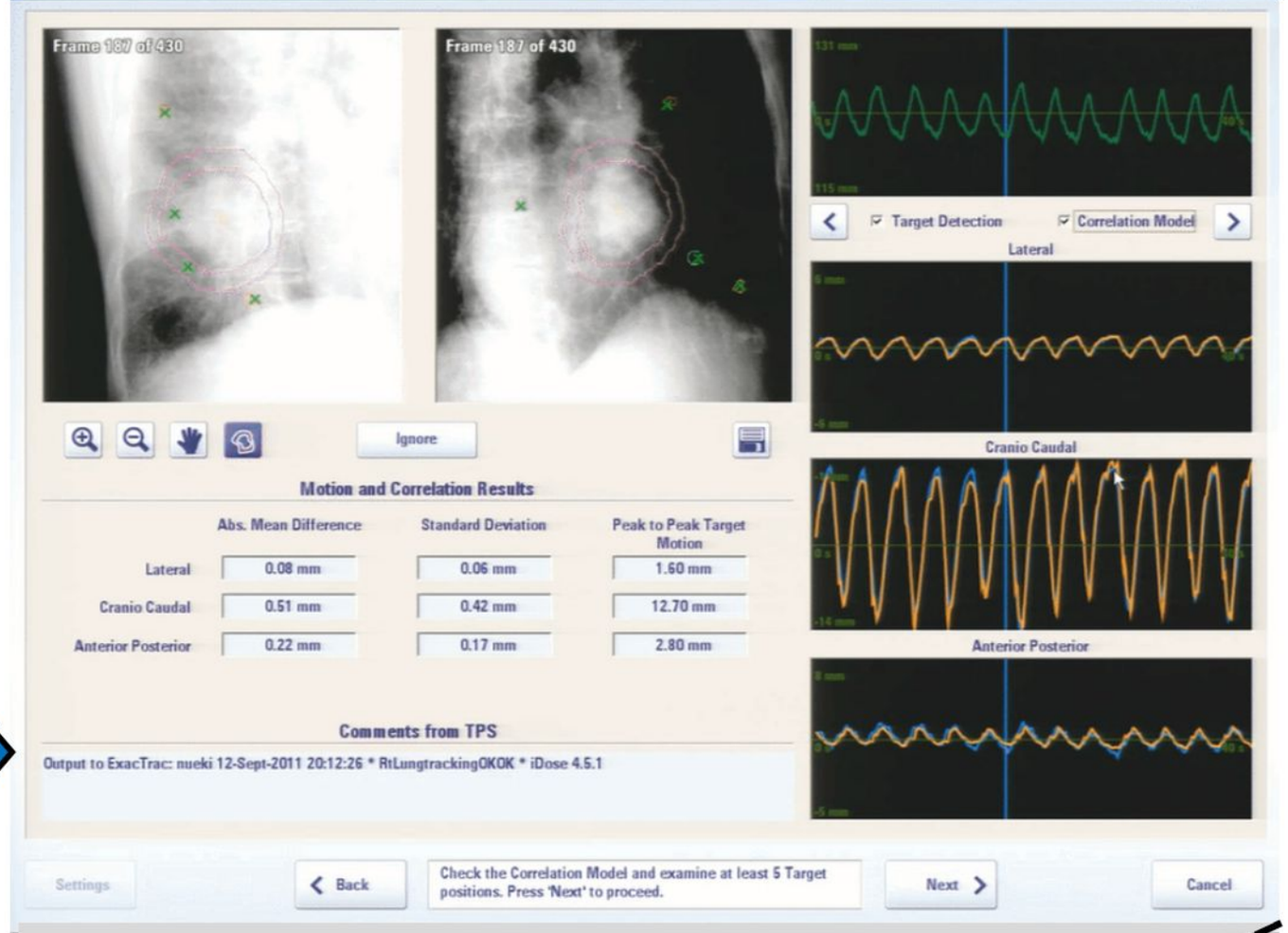

Irradiation phase

Monitoring IR marker position with IR camera on ExacTRAC

Calculating 3D target position by 4D model

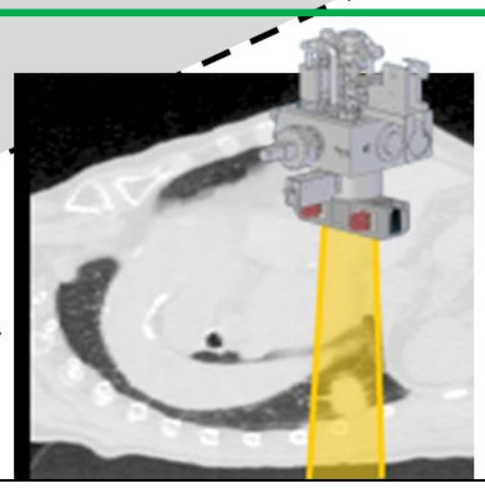

Dynamic tumor-tracking

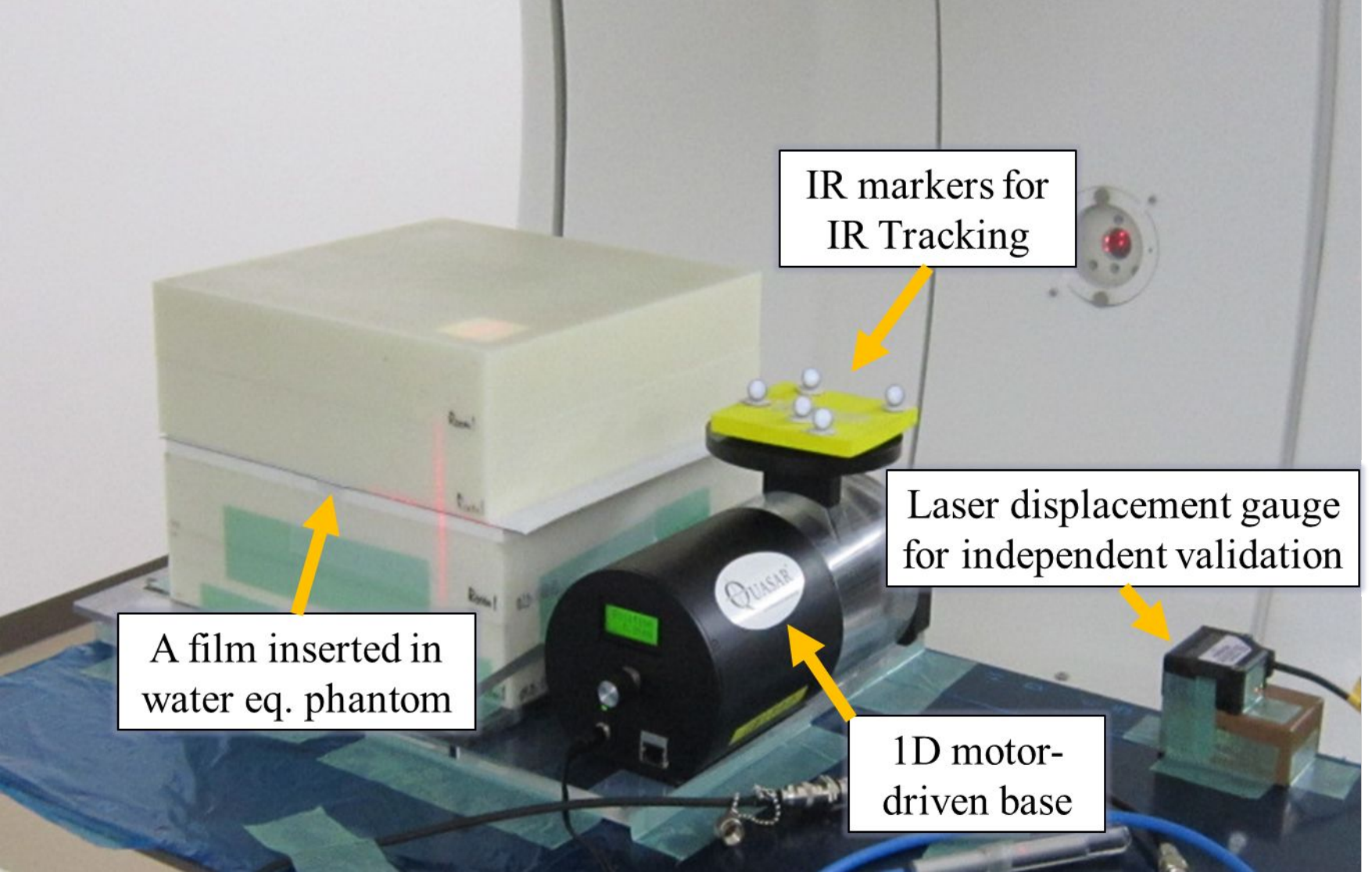
IR markers for
IR Tracking
Laser displacement gauge
for independent validation
A film inserted in
water eq. phantom
1D motor-
driven base

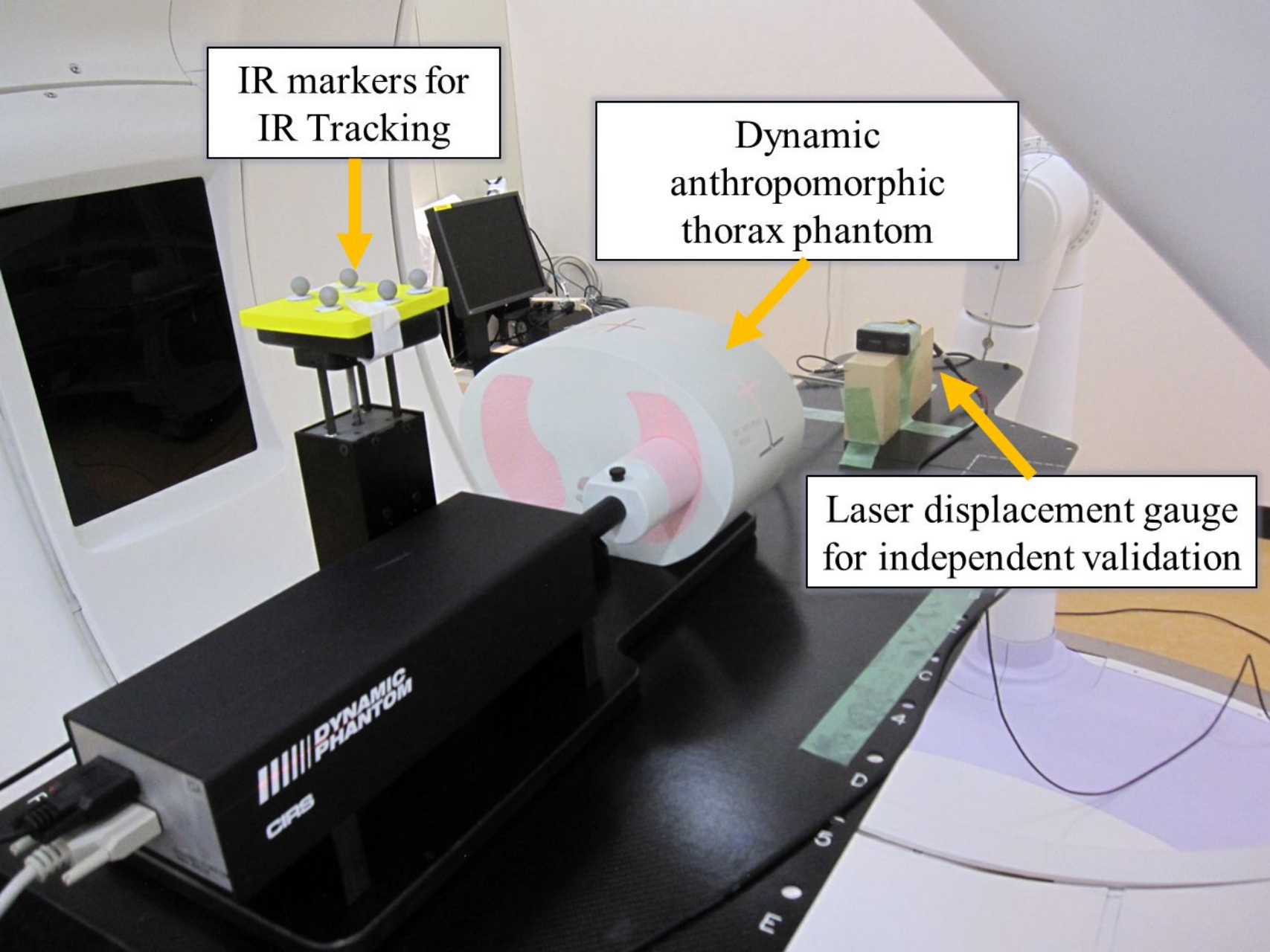
IR markers for IR Tracking
Dynamic anthropomorphic thorax phantom
Laser displacement gauge for independent validation
DYNAMIC PHANTOM
CIRS

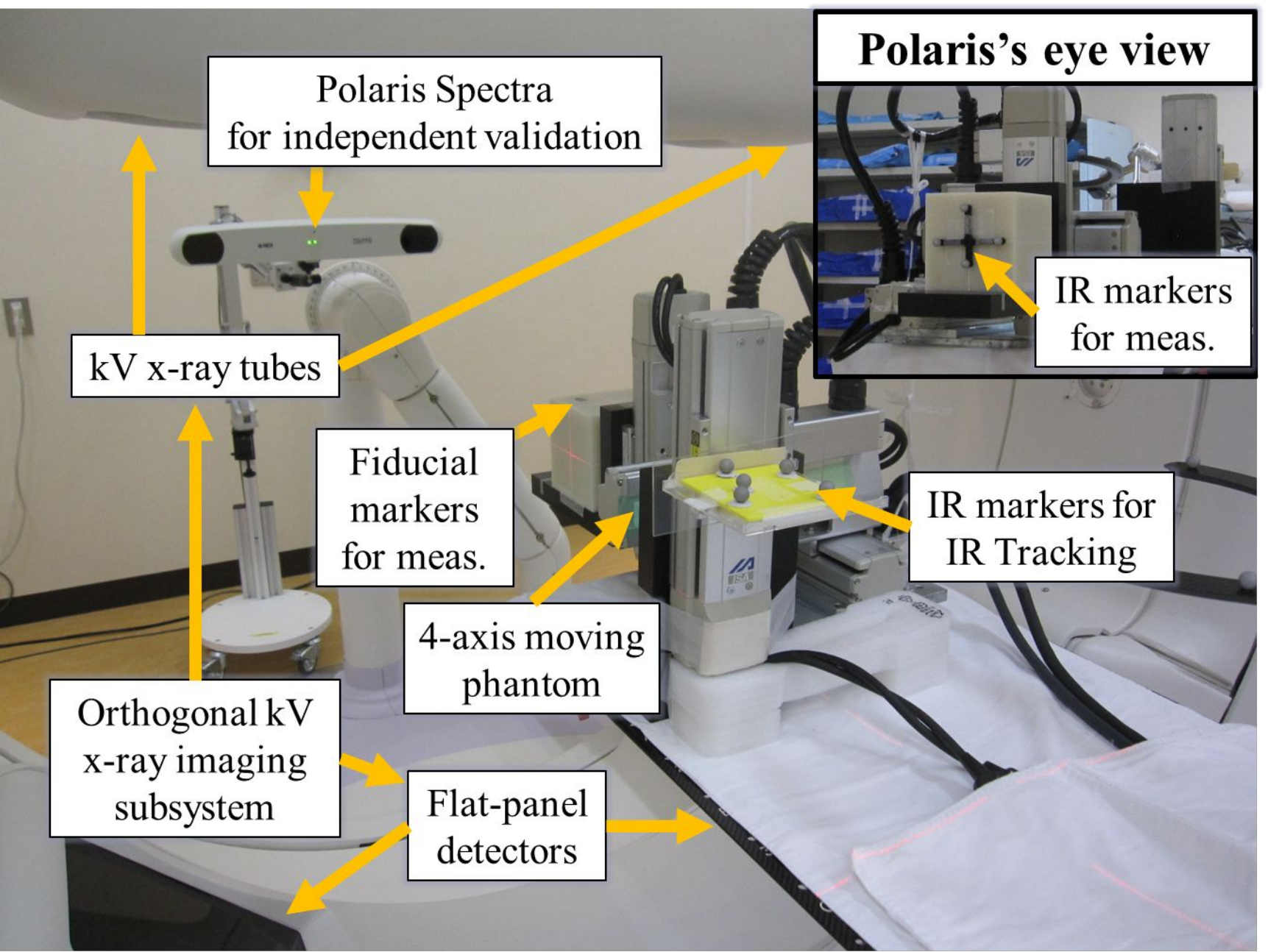
Polaris Spectra
for independent validation
Polaris's eye view
IR markers
for meas.
kV x-ray tubes
Fiducial
markers
for meas.
IR markers for
IR Tracking
4-axis moving
phantom
Orthogonal kV
x-ray imaging
subsystem
Flat-panel
detectors

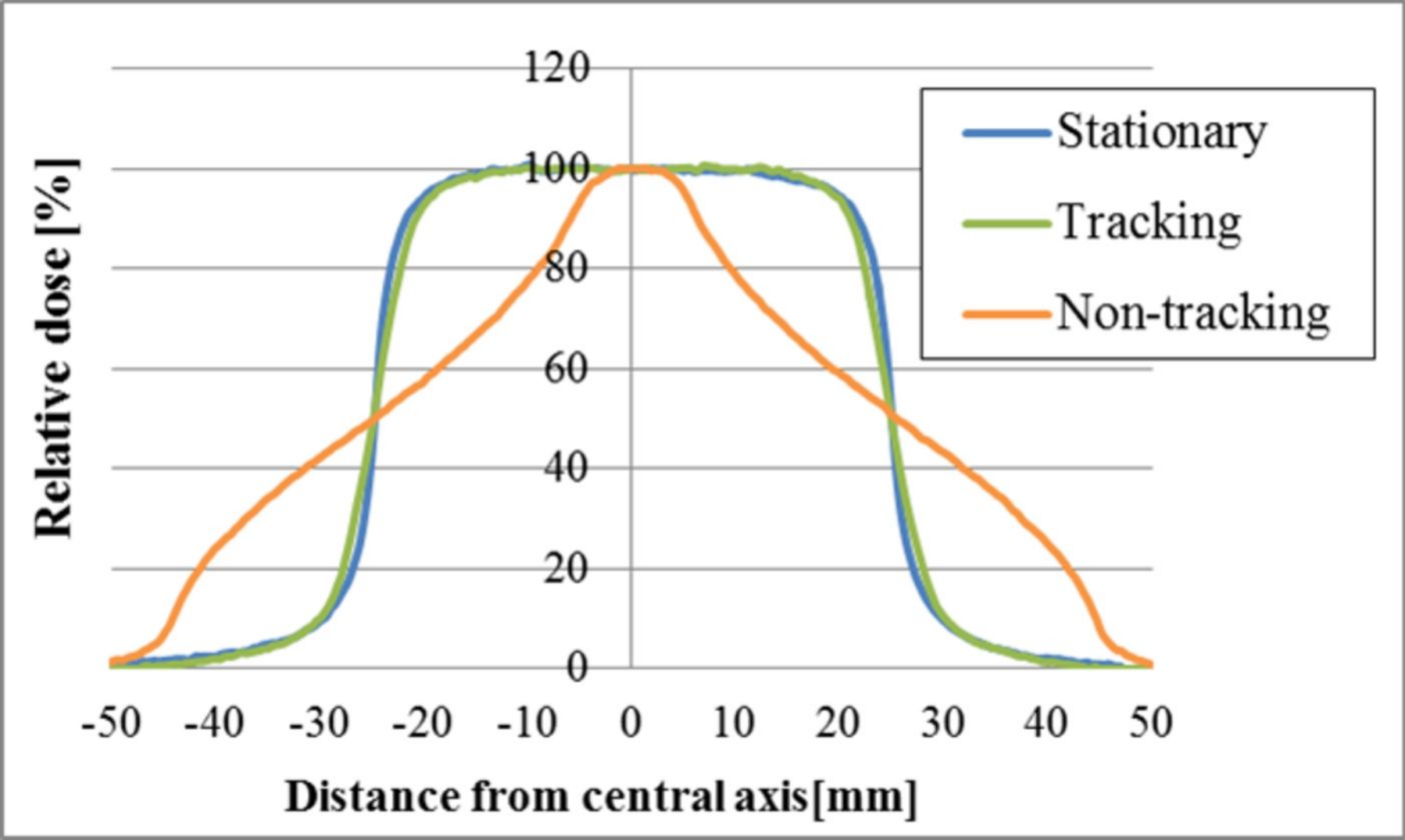
120
100
80
60
40
20
0
Relative dose [%]
-50
-40
-30
-20
-10
0
10
20
30
40
50
Distance from central axis[mm]
Stationary
Tracking
Non-tracking

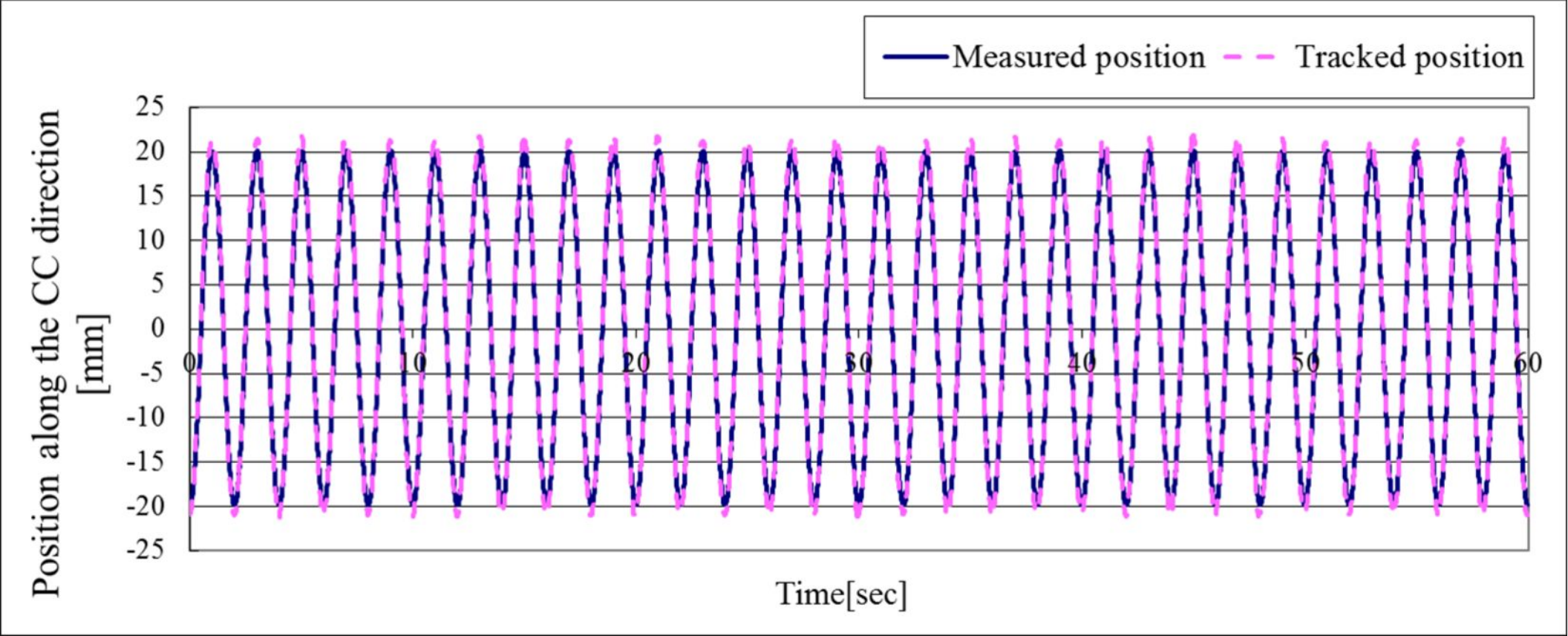
Measured position
Tracked position
Position along the CC direction [mm]
25
20
15
10
5
0
-5
-10
-15
-20
-25
0
10
20
30
40
50
60
Time[sec]

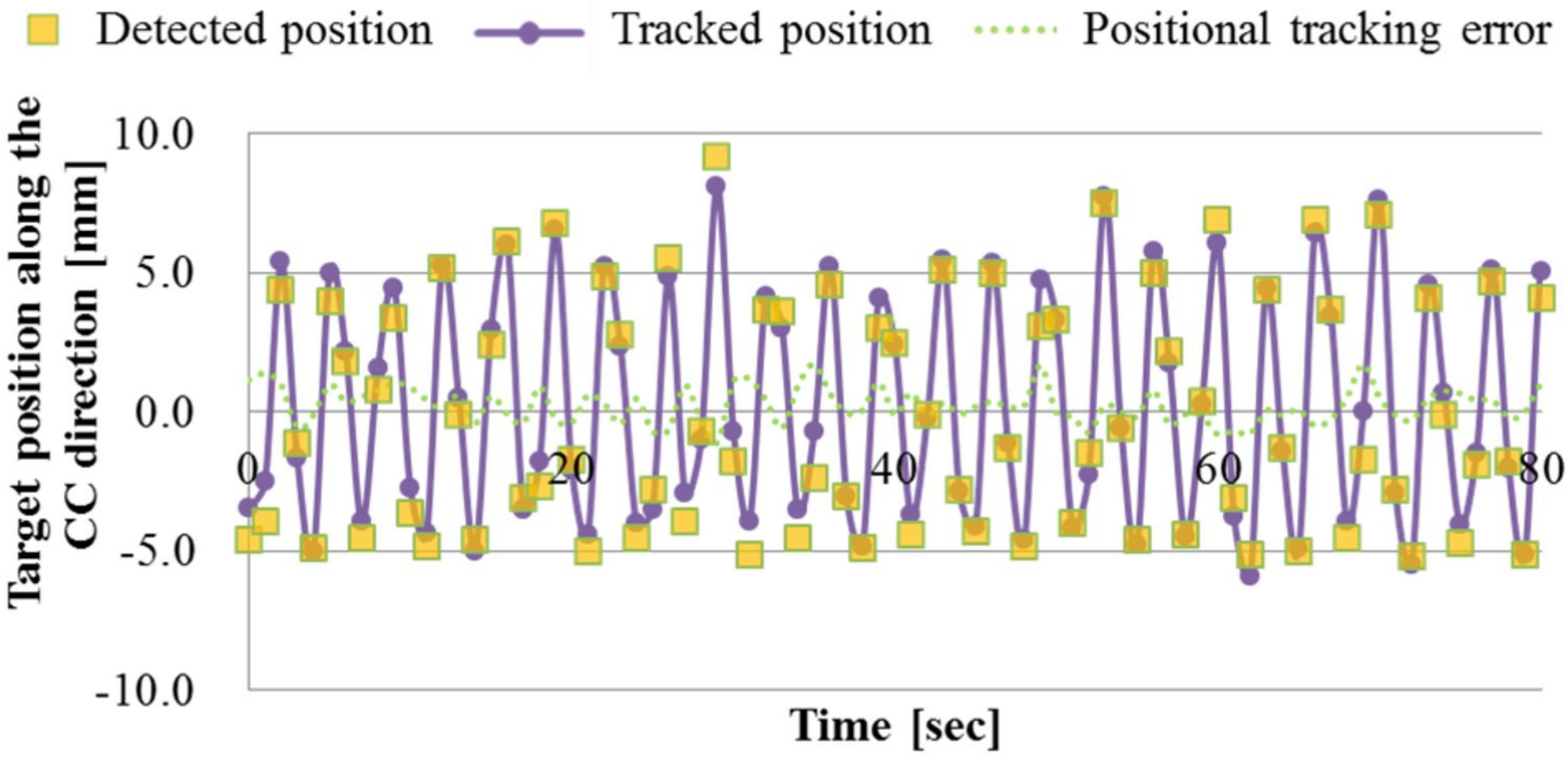
Detected position
Tracked position
Positional tracking error
Target position along the CC direction [mm]
10.0
5.0
0.0
-5.0
-10.0
0
20
40
60
80
Time [sec]

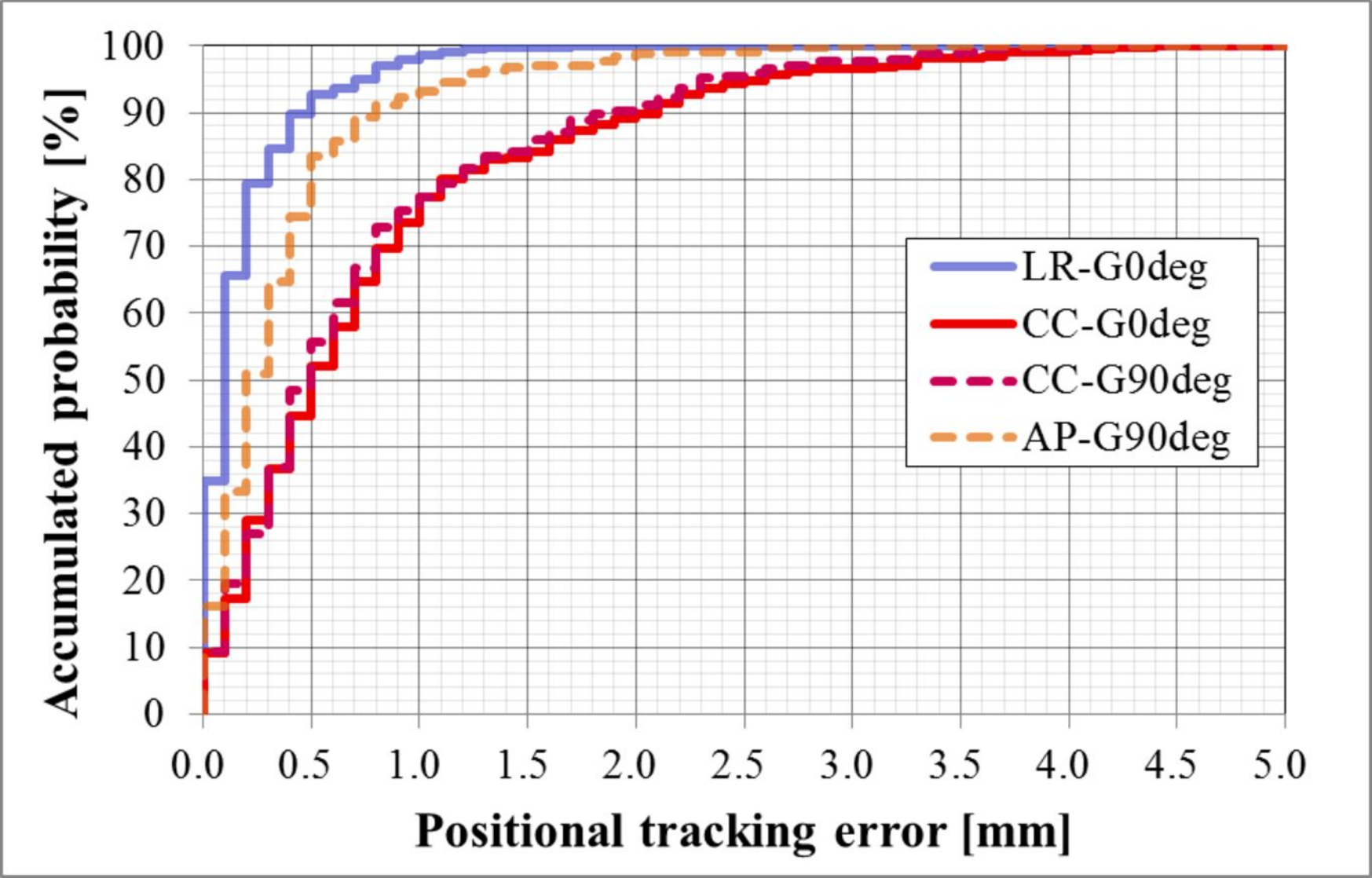
Accumulated probability [%]
100
90
80
70
60
50
40
30
20
10
0
0.0
0.5
1.0
1.5
2.0
2.5
3.0
3.5
4.0
4.5
5.0
Positional tracking error [mm]
LR-G0deg
CC-G0deg
CC-G90deg
AP-G90deg

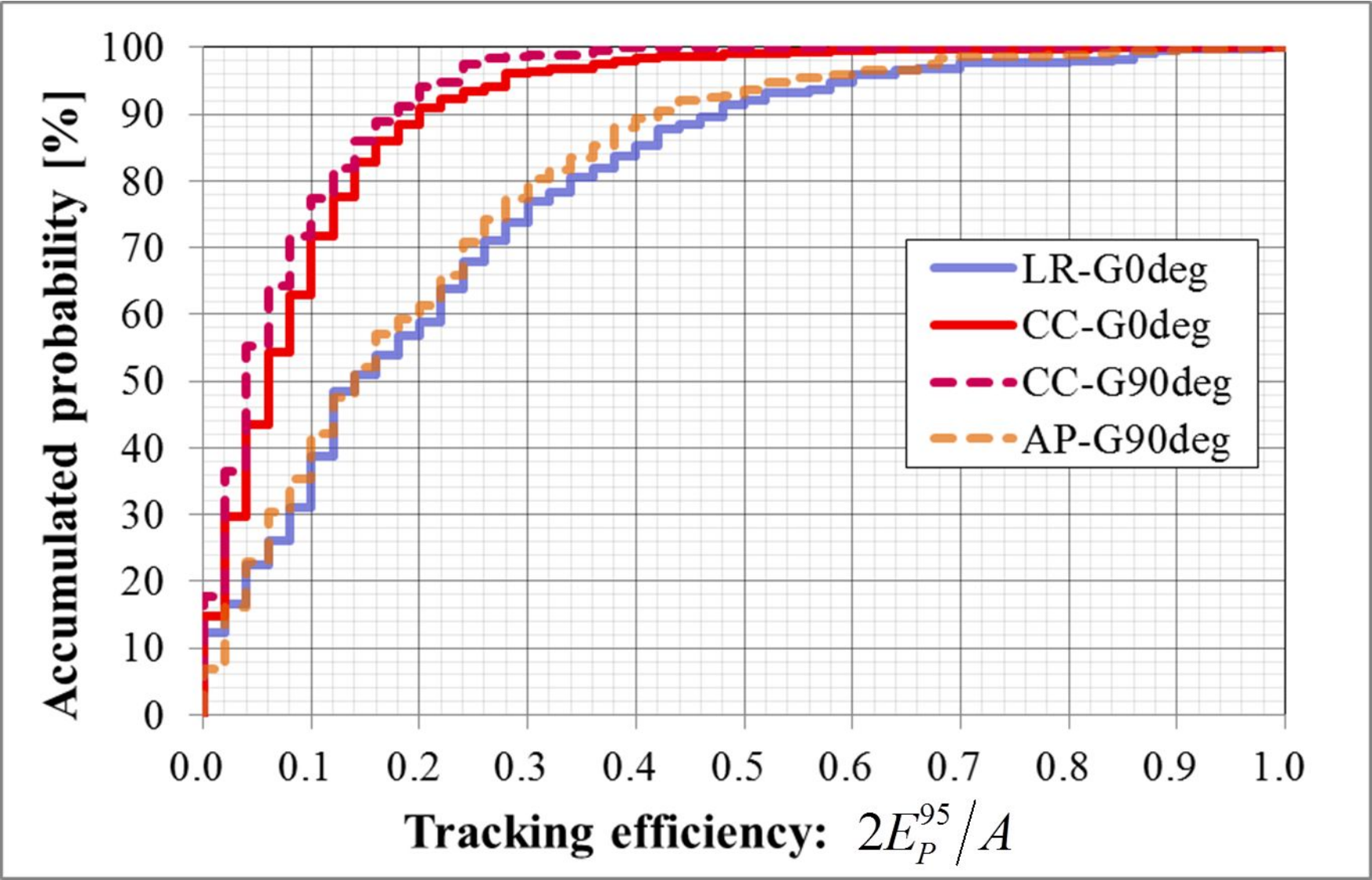
Accumulated probability [%]
100
90
80
70
60
50
40
30
20
10
0
0.0
0.1
0.2
0.3
0.4
0.5
0.6
0.7
0.8
0.9
1.0
Tracking efficiency: $2E_P^{95}/A$
LR-G0deg
CC-G0deg
CC-G90deg
AP-G90deg